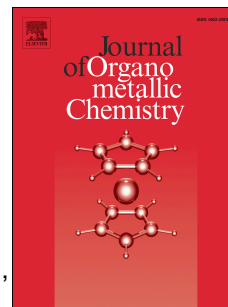


Accepted Manuscript

Neutral and cationic half-sandwich arene ruthenium, Cp*Rh and Cp*Ir oximato and oxime complexes: Synthesis, structural, DFT and biological studies

Sanjay Adhikari, Narasinga Rao Palepu, Dipankar Sutradhar, Samantha L. Shepherd, Roger M. Phillips, Werner Kaminsky, Asit K. Chandra, Mohan Rao Kollipara



PII: S0022-328X(16)30325-4

DOI: [10.1016/j.jorganchem.2016.08.004](https://doi.org/10.1016/j.jorganchem.2016.08.004)

Reference: JOM 19583

To appear in: *Journal of Organometallic Chemistry*

Received Date: 19 June 2016

Revised Date: 21 July 2016

Accepted Date: 2 August 2016

Please cite this article as: S. Adhikari, N.R. Palepu, D. Sutradhar, S.L. Shepherd, R.M. Phillips, W. Kaminsky, A.K. Chandra, M.R. Kollipara, Neutral and cationic half-sandwich arene ruthenium, Cp*Rh and Cp*Ir oximato and oxime complexes: Synthesis, structural, DFT and biological studies, *Journal of Organometallic Chemistry* (2016), doi: 10.1016/j.jorganchem.2016.08.004.

This is a PDF file of an unedited manuscript that has been accepted for publication. As a service to our customers we are providing this early version of the manuscript. The manuscript will undergo copyediting, typesetting, and review of the resulting proof before it is published in its final form. Please note that during the production process errors may be discovered which could affect the content, and all legal disclaimers that apply to the journal pertain.

1 Neutral and cationic half-sandwich arene ruthenium, Cp*Rh and Cp*Ir
2 oximato and oxime complexes: Synthesis, structural, DFT and biological
3 studies.

4
5
6 Sanjay Adhikari^a, Narasinga Rao Palepu^a, Dipankar Sutradhar^a, Samantha L
7 Shepherd^b, Roger M Phillips^b, Werner Kaminsky^c, Asit K. Chandra^a, Mohan Rao
8 Kollipara^{a*}

9
10 ^aCentre for Advanced Studies in Chemistry, North-Eastern Hill University, Shillong 793022,
11 India. E-mail: mohanrao59@gmail.com

12 Telephone Number: +91 364 2722620

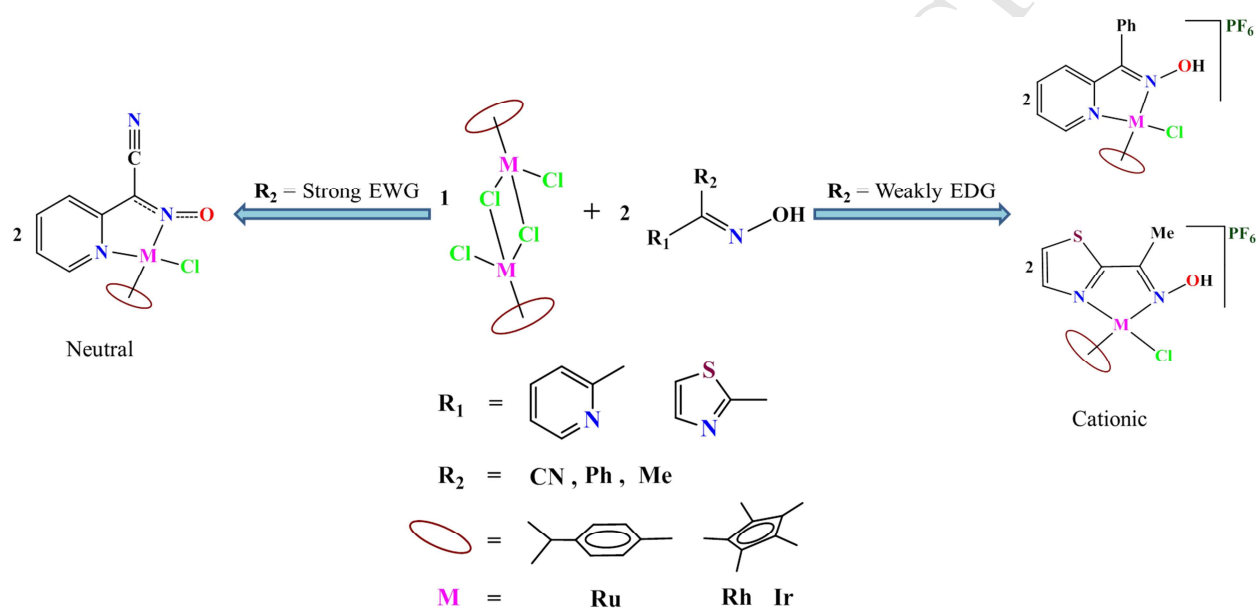
13 Fax Number: +91 364 2550076

14 ^bDepartment of Pharmacy, School of Applied Sciences, University of Huddersfield, Huddersfield
15 HD1 3DH, UK

16 ^cDepartment of Chemistry, University of Washington, Seattle, WA 98195, USA

17 **Graphical Abstract**

18 Reaction of strongly electron withdrawing cyano substituted pyridyl oxime with metal precursor
 19 afforded the neutral oximato metal complexes due to the deprotonation of the oxime hydrogen
 20 whereas reaction of weakly electron donating substituted phenyl and methyl oximes yielded
 21 cationic oxime complexes. The iridium complexes were found to be more active against
 22 MIAPaCa-2 cancer cell line.



23

24 Abstract

25 The reaction of [*p*-cymene)RuCl₂]₂ and [Cp**M*Cl₂]₂ (*M* = Rh/Ir) with chelating ligand 2-pyridyl
26 cyanoxime {pyC(CN)NOH} leads to the formation of neutral oximato complexes having the
27 general formula [(arene)*M*{pyC(CN)NO}Cl] {arene = *p*-cymene, *M* = Ru, **(1)**; Cp*, *M* = Rh **(2)**;
28 Cp*, *M* = Ir **(3)**}. Whereas the reaction of 2-pyridyl phenyloxime {pyC(Ph)NOH} and 2-
29 thiazolyl methyloxime {tzC(Me)NOH} with precursor compounds afforded the cationic oxime
30 complexes bearing formula [(arene)*M*{pyC(ph)NOH}Cl]⁺ and [(arene)*M*{tzC(Me)NOH}Cl]⁺
31 {arene = *p*-cymene *M* = Ru, **(4)**, **(7)**; Cp*, *M* = Rh **(5)**, **(8)**; Cp*, *M* = Ir **(6)**, **(9)**}. The cationic
32 complexes were isolated as their hexafluorophosphate salts. All these complexes were fully
33 characterized by analytical, spectroscopic and X-ray diffraction studies. The molecular structures
34 of the complexes revealed typical piano stool geometry around the metal center within which the
35 ligand acts as a NN' donor chelating ligand. The Chemo-sensitivity activities of the complexes
36 evaluated against HT-29 (human colorectal cancer), and MIAPaCa-2 (human pancreatic cancer)
37 cell line showed that the iridium-based complexes are much more potent than the ruthenium and
38 rhodium analogues. Theoretical studies were carried out to have a deeper understanding about
39 the charge distribution pattern and the various electronic transitions occurring in the complexes.

40 **Keywords:** Ruthenium, rhodium, iridium, oximes, cytotoxicity

41 1. Introduction

42 The study of half-sandwich arene ruthenium (arene = *p*-cymene and its derivatives)
43 Cp*Rh and Cp*Ir complexes represents one of the most versatile subject in the field of
44 organometallic chemistry because of their potential applications in various areas [1-6]. These
45 complexes bearing the general formula [(arene)(M)(L)X]⁺ (M = Ru, Rh and Ir, L is a chelating
46 ligand and X is a halide) have been extensively studied as potential metal-based anticancer drugs
47 [7-11]. The coordination sphere of the metal center in these half-sandwich complexes is
48 stabilized by the arene moiety which protects the metal's oxidation state occupying three
49 coordinating sites, the chelating ligand L which controls the reactivity through various
50 interactions and the M-Cl bond which easily gets dissociated and produces the active site for the
51 metal ion to target biomolecules [12, 13]. It is seen that the leaving group, the chelating ligand
52 and the arene substituent strongly influence the biological and structure activity relationship of
53 these complexes [14]. Sadler *et. al* carried out number of experiments with chelating N,N-, N,O-
54 and O,O- ligands to study the SAR activity of cytotoxic ruthenium(II) complexes by increasing
55 the size of the arene ring [15]. Also it has been proposed by various research groups that the
56 cytotoxicity of half-sandwich metal complexes increases with increase in size of the arene
57 substituent [16-18]. These complexes have also displayed their remarkable activity as catalyst in
58 various organic transformation reactions such as hydrogenation, water oxidation and C-H
59 activation [19-21]. In recent years many half-sandwich complexes with NN' chelating nitrogen
60 donor ligands have been accomplished in our laboratory [22].

61 Oxime ligands in particular have developed a keen interest in the field of coordination
62 chemistry [23]. The oxime ligand can act as an ambidentate ligand and can coordinate with metal
63 ions either through nitrogen or oxygen atoms [24]. Cyanoximes having the general formula

64 {HO-N=C(CN)-R}, where R is an electron withdrawing group represents an important class of
65 biologically active compounds and transition metal complexes of cyanoximes have shown
66 pronounced cytotoxicity and antimicrobial activity [25, 26]. The presence of the cyano group as
67 a substituent close to the oxime fragment increases the acidity of the oxime several thousand
68 times greater than that of common oximes [27]. The anions of 2-pyridyl oximes serve as a
69 versatile ligand for preparation of complexes with unusual topologies exhibiting interesting
70 magnetic properties [28]. Oximes have the capability to remain intact in the co-ordination sphere
71 of the metal by undergoing O-H bond cleavage to afford oximate derivatives [29]. Despite
72 having a rich diversified chemistry of metal oxime and oximate complexes, it is noteworthy that
73 only a few half-sandwich platinum group metal oxime complexes have been reported to date [30,
74 31].

75 In our present work we report the synthesis of ruthenium, rhodium and iridium half-
76 sandwich oximate and oxime complexes, their biological activity and theoretical studies.
77 Ligands used in the present study are shown in Chart-1.

78 **2 Experimental**

79 *2.1. Materials and methods*

80 All reagents were purchased from commercial sources and used as received without
81 further purification. RuCl₃.nH₂O, RhCl₃.nH₂O, IrCl₃.nH₂O was purchased from Arora Matthey
82 limited. 2-acetylthiazole and 2-benzoylpyridine were obtained from Aldrich, 2-
83 pyridylacetonitrile was obtained from Alfa Aesar and hydroxylamine hydrochloride was
84 obtained from himedia. The solvents were purified and dried according to standard procedures
85 [32]. The starting precursor metal complexes [(*p*-cymene)RuCl₂]₂ and [Cp*MCl₂]₂ (M = Rh/Ir)
86 were prepared according to the literature methods [33, 34]. The oxime ligands 2-pyridyl

87 cyanoxime, 2-pyridyl phenyloxime and 2-thiazolyl methyloxime were synthesized according to
88 published procedures [29, 35 and 36]. Infrared spectra were recorded on a Perkin-Elmer 983
89 spectrophotometer by using KBr pellets in the range of 400-4000 cm^{-1} . ^1H NMR spectra were
90 recorded on a Bruker Avance II 400 MHz spectrometer using DMSO-d_6 as solvents. Absorption
91 spectra were recorded on a Perkin-Elmer Lambda 25 UV/Vis spectrophotometer in the range of
92 200-800 nm at room temperature in acetonitrile. Mass spectra were recorded using Q-ToF APCI-
93 MS instrument (model HAB 273). Elemental analyses of the complexes were performed on a
94 Perkin-Elmer 2400 CHN/S analyzer.

95 2.2. *Structure determination by X-ray crystallography*

96 Suitable single crystals of complexes (1), (2) and (3), were obtained by slow diffusion of
97 hexane into acetone solution and crystals of complexes (4), (5), (7) and (8) were obtained by
98 diffusing hexane into DCM solution. Single crystal X-ray diffraction data for the complexes
99 were collected on an Oxford Diffraction Xcalibur Eos Gemini diffractometer at 293 K using
100 graphite monochromated $\text{Mo-K}\alpha$ radiation ($\lambda = 0.71073 \text{ \AA}$). The strategy for the data collection
101 was evaluated using the CrysAlisPro CCD software. Crystal data were collected by standard
102 ‘‘phi-omega scan’’ techniques and were scaled and reduced using CrysAlisPro RED software.
103 The structures were solved by direct methods using SHELXS-97 and refined by full-matrix least
104 squares with SHELXL-97 refining on F^2 [37, 38]. The positions of all the atoms were obtained
105 by direct methods. Metal atoms in the complex were located from the E-maps and non-hydrogen
106 atoms were refined anisotropically. The hydrogen atoms bound to the carbon were placed in
107 geometrically constrained positions and refined with isotropic temperature factors, generally 1.2
108 U_{eq} of their parent atoms. Crystallographic and structure refinement parameters for the
109 complexes are summarized in Table 1, and selected bond lengths and bond angles are presented

110 in Table 2. Figures 1-3 were drawn with ORTEP3 program whereas Figures S2-S6 was drawn by
111 using MERCURY 3.6 program [39].

112 The crystal structure of complex (5) contains disordered hexane molecule, which has
113 been removed by SQUEEZE method [40]. Crystal structure of complex (6) contains fourfold
114 disordered solvent molecule, which has been refined and removed by SQUEEZE method.
115 Crystal structure of complex (8) contains solvent molecule in their solved structure.

116 2.3. *Biological studies*

117 The complexes (1-9) were dissolved in DMSO at 100 mM and stored at -20 °C until
118 required. The cytotoxicity of the complexes was studied against HT-29 (human colorectal
119 cancer) and MIA PaCa-2 (human pancreatic cancer) cell line. Cells were seeded into 96 well
120 plates at 1×10^3 cells per well and incubated at 37 °C in a CO₂ enriched (5%), humidified
121 atmosphere overnight to adhere. The cells were exposed to a range of drug concentrations in the
122 range of 0-100 μM for four days before cell survival was determined using the MTT assay [41].
123 To each well MTT (0.5 mg/ml) in phosphate buffered saline was added and was further
124 incubated at 37 °C for 4 hours. The MTT was then removed from each well and the formazan
125 crystals formed were dissolved in 150 μM DMSO and the absorbance of the resulting solution
126 was recorded at 550 nm using an ELISA spectrophotometer. The percentage of cell inhibition
127 was calculated by dividing the absorbance of treated cell by the control value absorbance
128 (exposed to 0.1 % DMSO). The IC₅₀ values were determined from plots of % survival against
129 drug concentration. Each experiment was repeated three times and a mean value obtained and
130 stated as IC₅₀ (μM) ± SD.

131 2.4. *Computational Methodology*

132 The geometry optimization of all the complexes were done in the gas phase using the
133 Density Functional Theory (DFT) based B3LYP method in conjugation with 6-31G** basis set
134 for lighter atoms (H, C, N, O, Cl, S, P and F) and LANL2DZ [42, 43] basis set for heavier atoms
135 (Ru, Rh and Ir). LANL2DZ is a widely used Effective Core Potential (ECP) basis set which
136 considers the core electrons as chemically inactive and performs only on the valence electrons
137 and thus reduces the computational cost. Harmonic frequency calculations were carried out at the
138 same level to ensure that the geometries are minima at the potential energy surface (PES).
139 Natural Bond Orbital (NBO) [44] analysis was carried out to get charges on individual atoms
140 present in the complexes. Time dependent-Density Functional Theory (TD-DFT) [45] has been
141 employed to evaluate the absorption spectra and the electronic transitions of the metal
142 complexes. In order to incorporate the effect of the solvent around the molecule, the Polarizable
143 Continuum Model (PCM) [46] was used in TD-DFT calculations. The composition of the
144 molecular orbital analysis was carried out using the Chemissian software package [47]. All the
145 electronic energy calculations were carried out using Gaussian 09 suite of program [48].

146 2.5. *General procedure for synthesis of neutral complexes (1-3)*

147 A mixture of starting metal precursor (0.1 mmol) and ligand 2-pyridyl cyanoxime,
148 {pyC(CN)NOH} (0.2 mmol) were dissolved in dry methanol (10 ml) and stirred at room
149 temperature for 8 hours (Scheme-1). A yellow colored compound precipitated out from the
150 reaction mixture. The precipitate was filtered, washed with cold methanol (2 x 5 ml) and diethyl
151 ether (3 x 10 ml) and dried in vacuum.

152 2.5.1. *[(p-cymene)Ru{pyC(CN)NO}Cl] (1)*

153 Yield: 62 mg (74%); IR (KBr, cm^{-1}): 2959(m), 2203(m), 1603(m), 1482(m), 1443(m), 1396(s),
 154 1368(m), 871(m), 788(m); ^1H NMR (400 MHz, DMSO-d_6): δ = 9.20 (d, 1H, J = 8.0 Hz, $\text{CH}_{(\text{py})}$),
 155 7.94 (t, 1H, $\text{CH}_{(\text{py})}$), 7.38 (t, 1H, $\text{CH}_{(\text{py})}$), 7.30 (d, 1H, J = 8.0 Hz, $\text{CH}_{(\text{py})}$), 1.01 (dd, 6H, J = 8 and
 156 8 Hz, $\text{CH}_{(p\text{-cym})}$), 2.07 (s, 3H, $\text{CH}_{(p\text{-cym})}$), 2.62 (sept, 1H, $\text{CH}_{(p\text{-cym})}$), 5.60 (d, 1H, J = 8.0 Hz, $\text{CH}_{(p\text{-cym})}$),
 157 5.68 (d, 1H, J = 4.0, $\text{CH}_{(p\text{-cym})}$), 5.80 (d, 1H, J = 8.0, $\text{CH}_{(p\text{-cym})}$), 5.87 (d, 1H, J = 8.0 Hz,
 158 $\text{CH}_{(p\text{-cym})}$); HRMS-APCI (m/z): 417.0302 ($\text{M}+\text{H}$) $^+$; UV-Vis { Acetonitrile, λ_{max} nm ($\epsilon/10^{-4}$ M^{-1}
 159 cm^{-1})}: 237 (1.83), 302 (1.18), 370 (0.61); Anal. Calc for $\text{C}_{17}\text{H}_{18}\text{ClN}_3\text{ORu}$ (416.86); C, 48.98; H,
 160 4.35; N, 10.08. Found: C, 49.14; H, 4.42; N, 10.23 %.

161 2.5.2. [$\text{Cp}^*\text{Rh}\{\text{pyC}(\text{CN})\text{NO}\}\text{Cl}$] (2)

162 Yield: 66 mg (78%); IR (KBr, cm^{-1}): 2918(m), 2212(m), 1602(m), 1481(m), 1444(m), 1398(s),
 163 1372(s), 1155(m), 766(m); ^1H NMR (400 MHz, DMSO-d_6): δ = 8.54 (d, 1H, J = 4.0 Hz, $\text{CH}_{(\text{py})}$),
 164 7.88 (t, 1H, $\text{CH}_{(\text{py})}$), 7.40 (t, 1H, $\text{CH}_{(\text{py})}$), 7.31 (d, 1H, J = 8.0 Hz, $\text{CH}_{(\text{py})}$), 1.59 (s, 15H, $\text{CH}_{(\text{Cp}^*)}$);
 165 HRMS-APCI (m/z): 420.0451 ($\text{M}+\text{H}$) $^+$; UV-Vis { Acetonitrile, λ_{max} nm ($\epsilon/10^{-4}$ M^{-1} cm^{-1})}: 236
 166 (1.78), 255 (1.35), 289 (1.08), 374 (0.71); Anal. Calc for $\text{C}_{17}\text{H}_{19}\text{ClN}_3\text{ORh}$ (419.71); C, 48.65; H,
 167 4.56; N, 10.01. Found: C, 48.68; H, 4.62; N, 10.18 %.

168 2.5.3. [$\text{Cp}^*\text{Ir}\{\text{pyC}(\text{CN})\text{NO}\}\text{Cl}$] (3)

169 Yield: 80 mg (78%); IR (KBr, cm^{-1}): 2922(m), 2204(m), 1605(w), 1483(m), 1394(s), 1368(s),
 170 765(m); ^1H NMR (400 MHz, DMSO-d_6): δ = 8.54 (d, 1H, J = 4.0 Hz, $\text{CH}_{(\text{py})}$), 7.80 (t, 1H,
 171 $\text{CH}_{(\text{py})}$), 7.52 (d, 1H, J = 4 Hz, $\text{CH}_{(\text{py})}$), 7.23 (t, 1H, $\text{CH}_{(\text{py})}$), 1.62 (s, 15H, $\text{CH}_{(\text{Cp}^*)}$); HRMS-APCI
 172 (m/z): 510.0824 ($\text{M}+\text{H}$) $^+$; UV-Vis { Acetonitrile, λ_{max} nm ($\epsilon/10^{-4}$ M^{-1} cm^{-1})}: 233 (1.46), 288
 173 (0.96), 378 (0.53); Anal. Calc for $\text{C}_{17}\text{H}_{19}\text{ClN}_3\text{OIr}$ (509.02); C, 40.11; H, 3.76; N, 8.26. Found: C,
 174 40.28; H, 3.88; N, 8.38 %.

175 2.6. General procedure for synthesis of cationic complex (4-9)

176 A mixture of starting metal precursor (0.1 mmol) and ligand 2-pyridyl phenyloxime
177 {pyC(Ph)NOH} or 2-thiazolyl methyloxime {tzC(Me)NOH} (0.2 mmol) and 2.5 equivalents of
178 NH_4PF_6 were dissolved in dry methanol (10 ml) and stirred at room temperature for 8 hours
179 (Scheme-2 and 3). The solvent was evaporated the residue was dissolved in dichloromethane and
180 filtered through celite, the filtrate was concentrated to 1 ml and excess hexane was added to
181 precipitate the compound. The precipitate was collected and dried in vacuum.

182 2.6.1. [(*p*-cymene)Ru{pyC(Ph)NOH}Cl](PF₆) (4)

183 Yield: 96 mg (78%); IR (KBr. cm^{-1}): 3314(b), 3090(s), 2967(w), 1598(s), 1472(s), 1366(m),
184 1192(s), 1031(s) 838(s); ^1H NMR (400 MHz, DMSO- d_6): 9.45 (d, 1H, $J = 8.0$ Hz, $\text{CH}_{(\text{py})}$), 8.04
185 (t, 1H, $\text{CH}_{(\text{py})}$), 7.66 (t, 1H, $\text{CH}_{(\text{py})}$), 7.54-7.59 (m, 3H, $\text{CH}_{(\text{py})}$, (Ar)), 7.29-7.32 (m, 3H, $\text{CH}_{(\text{Ar})}$),
186 1.06 (d 3H, $J = 8.0$ Hz, $\text{CH}_{(p\text{-cym})}$), 1.13 (d, 3H, $J = 8.0$ Hz, $\text{CH}_{(p\text{-cym})}$), 2.26 (s, 3H, $\text{CH}_{(p\text{-cym})}$),
187 2.70 (sept, 1H, $\text{CH}_{(p\text{-cym})}$), 5.72 (d, 1H, $J = 8.0$ Hz, $\text{CH}_{(p\text{-cym})}$), 6.02 (d, 1H, $J = 8.0$ Hz, $\text{CH}_{(p\text{-cym})}$),
188 6.12 (d, 1H, $J = 8.0$ Hz, $\text{CH}_{(p\text{-cym})}$), 6.19 (d, 1H, $J = 8.0$ Hz, $\text{CH}_{(p\text{-cym})}$), OH not observed; HRMS-
189 APCI (m/z): 469.0652 (M-PF₆)⁺; UV-Vis {Acetonitrile, λ_{max} nm ($\epsilon/10^{-4}$ M⁻¹ cm⁻¹): 233 (2.28),
190 272 (0.95), 376 (0.29); Anal. Calc for C₂₂H₂₄ClF₆N₂OPRu (613.93); C, 43.04; H, 3.94; N, 4.56.
191 Found: C, 43.21; H, 4.06; N, 4.63 %.

192 2.6.2. [Cp*Rh{pyC(Ph)NOH}Cl](PF₆) (5)

193 Yield: 108 mg (87%); IR (KBr. cm^{-1}): 3314(b), 3112(m), 2922(m), 1595(s), 1470(w), 1378(w),
194 1189(s), 1027(s), 841(s); ^1H NMR (400 MHz, DMSO- d_6): $\delta = 8.77$ (d, 1H, $J = 4.0$ Hz, $\text{CH}_{(\text{py})}$),
195 8.06 (t, 1H, $\text{CH}_{(\text{py})}$), 7.77 (t, 1H, $\text{CH}_{(\text{py})}$), 7.59-7.63 (m, 3H, $\text{CH}_{(\text{py})}$, (Ar)), 7.40-7.45 (m, 3H,
196 $\text{CH}_{(\text{Ar})}$), 1.77 (s, 15 H, $\text{CH}_{(\text{Cp}^*)}$), OH not observed; HRMS-APCI (m/z): 471.0721 (M-PF₆)⁺; UV-
197 Vis {Acetonitrile, λ_{max} nm ($\epsilon/10^{-4}$ M⁻¹ cm⁻¹): 266 (0.75), 357 (0.30); Anal. Calc for
198 C₂₂H₂₅ClF₆N₂OPRh (616.77); C, 42.84; H, 4.09; N, 4.54. Found: C, 42.91; H, 3.96; N, 4.67 %.

199 **2.6.3. [*Cp*Ir*{*pyC(Ph)NOH*}*Cl*](*PF*₆) (6)**

200 Yield: 110 mg (78%); IR (KBr. cm⁻¹): 3438(b), 3137(m), 2975(m), 1624(s), 1457(w), 1378(w),
 201 1142(s), 1033(s), 843(s); ¹H NMR (400 MHz, DMSO-d₆): δ = 8.78 (d, 1H, *J* = 4.0 Hz, CH_(py)),
 202 7.92 (t, 1H, CH_(py)), 7.79 (t, 1H, CH_(py)), 7.48-7.53 (m, 3H, CH_(py), (Ar)), 7.43-7.47 (m, 3H,
 203 CH_(Ar)), 1.77 (s, 15 H, CH_(Cp*)), OH not observed; HRMS-APCI (m/z): 561.1283 (M-PF₆)⁺; UV-
 204 Vis {Acetonitrile, λ_{max} nm (ε/10⁻⁴ M⁻¹ cm⁻¹)}: 296 (0.78), 360 (0.59); Anal. Calc for
 205 C₂₂H₂₅ClF₆N₂OPIr (706.08); C, 37.42; H, 3.57; N, 3.97. Found: C, 37.58; H, 3.65; N, 4.11 %.

206 **2.6.4. [*(p-cymene)Ru*{*tz(CH*₃*)NOH*}*Cl*](*PF*₆) (7)**

207 Yield: 88 mg (79%); IR (KBr. cm⁻¹): 3594(s), 3429(b), 3109(m), 2970(m), 1631(s), 1505(m),
 208 1471(w), 1381(s), 1140(s), 1040(m), 846(s); ¹H NMR (400 MHz, DMSO-d₆): δ = 11.3 (s, 1H,
 209 OH), 8.50 (d, 1H, *J* = 4.0 Hz, CH_(tz)) 7.89 (d, 1H, *J* = 8.0 Hz, CH_(tz)), 2.52 (s, 3H, CH₃), 1.10 (d,
 210 3H, *J* = 8 Hz, CH_(p-cym)), 1.18 (d, 1H, *J* = 8 Hz, CH_(p-cym)), 2.29 (s, 3H, CH_(p-cym)), 2.75 (sept, 1H),
 211 6.06 (d, 1H, *J* = 4 Hz, CH_(p-cym)), 5.89 (d, 2H, *J* = 8 Hz, CH_(p-cym)), 5.64 (d, 1H, *J* = 4 Hz, CH_{(p-}
 212 _{cym)}); HRMS-APCI (m/z): 413.0118 (M-PF₆)⁺; UV-Vis {Acetonitrile, λ_{max} nm (ε/10⁻⁴ M⁻¹ cm⁻¹)}:
 213 297 (0.48), 350 (0.32); Anal. Calc for C₁₅H₂₀ClF₆N₂OPRuS (557.88); C, 32.29; H, 3.61; N, 5.02.
 214 Found: C, 32.41; H, 3.69; N, 5.13 %.

215 **2.6.5. [*Cp*Rh*{*tzC(CH*₃*)NOH*}*Cl*](*PF*₆) (8)**

216 Yield: 84 mg (75%); IR (KBr. cm⁻¹): 3618(s), 3433(b), 3138(m), 2824(w), 1598(s), 1470(w),
 217 1382(w), 1139(m), 1027(w), 842(s); ¹H NMR (400 MHz, DMSO-d₆): δ = 11.81 (s, 1H, OH),
 218 8.14 (d, 1H, *J* = 4 Hz, CH_(tz)), 8.08 (d, 1H, *J* = 4 Hz, CH_(tz)), 2.56 (s, 3H, CH₃), 1.78 (s, 15 H,
 219 CH_(Cp*)); HRMS-APCI (m/z): 415.0131 (M-PF₆)⁺; UV-Vis { Acetonitrile, λ_{max} nm (ε/10⁻⁴ M⁻¹
 220 cm⁻¹)}: 230 (0.53), 287 (0.35), 351 (0.32); Anal. Calc for C₁₅H₂₁ClF₆N₂OPRhS (560.73); C,
 221 32.13; H, 3.77; N, 5.00. Found: C, 32.19; H, 3.85; N, 5.12 %.

222 **2.6.6. [Cp*Ir{tzC(CH₃)NOH}Cl](PF₆) (9)**

223 Yield: 100 mg (77%); IR (KBr. cm⁻¹): 3619(s), 3339(b), 3136(m), 2926(m), 1599(m), 1458(m),
224 1387(m), 1144(w), 1036(m), 844(s); ¹H NMR (400 MHz, DMSO-d₆): δ = 11.81 (s, 1H, OH),
225 8.25 (d, 1H, *J* = 4 Hz, CH_(tz)), 8.23 (d, 1H, *J* = 4 Hz, CH_(tz)), 2.58 (s, 3H, CH₃), 1.77 (s, 15 H,
226 CH_(Cp*)); HRMS-APCI (m/z): 505.0761 (M-PF₆)⁺; UV-Vis {Acetonitrile, λ_{max} nm (ε/10⁻⁴ M⁻¹ cm⁻¹
227 ¹): 290 (0.76), 360 (0.346); Anal. Calc for C₁₅H₂₁ClF₆N₂OPIrS (650.04); C, 27.72; H, 3.26; N,
228 4.31. Found: C, 27.90; H, 3.32; N, 4.41 %.

229 **3. Results and discussion**

230 *3.1. Synthesis of the complexes*

231 The neutral metal oximate complexes (**1-3**) were isolated by the reaction of metal
232 precursors with 2-pyridyl cyanoxime. The neutral metal complexes were formed as a result of
233 deprotonation of the oxime hydrogen as confirmed by spectroscopic and X-ray diffraction
234 studies. It is assumed that the presence of the cyano group as a substituent in 2-pyridyl
235 cyanoxime increases its acidity leading to its deprotonation and resulting in elimination of HCl.
236 Furthermore deprotonation of oxime hydrogen generates an anionic charge on oxime-O which
237 was found to be delocalized over the 2-pyridyl cyanoxime moiety as reflected from the bond
238 lengths values (Table 2). The cationic metal oxime complexes (**4-9**) were prepared by the
239 reaction of metal precursors with 2-pyridyl phenyloxime and 2-thiazolyl methyloxime.
240 Deprotonation of oxime hydrogen was not observed in this case with phenyl and methyl as
241 substituent. The cationic complexes were isolated with PF₆ counter ion. All these complexes
242 were isolated as yellow solids except complexes (**6** and **9**) which were isolated as orange solids.
243 These complexes are non-hygroscopic, stable in air as well as in solid state. They are soluble in
244 common organic solvents like acetone, acetonitrile, dichloromethane and DMSO but insoluble in

245 hexane and diethyl ether. All these complexes were fully characterized by spectroscopic
246 techniques.

247 3.2. Spectral studies of the complexes

248 The IR spectra of all the complexes shows characteristic stretching frequencies for C=N
249 and C=C around 1450-1620 cm^{-1} and these values are shifted to higher frequencies as compared
250 to the free ligand following coordination of the ligand to the metal atom. The C \equiv N stretching
251 frequencies for the neutral complexes (**1-3**) appeared in the lower frequency region around 2204-
252 2212 cm^{-1} as compared to the free ligand at 2229 cm^{-1} which may be due to delocalization of the
253 anionic charge on oxime-O. The disappearance of the OH stretching frequency around 3100-
254 3400 cm^{-1} in the neutral complexes (**1-3**) indicates the deprotonation of the oxime hydrogen,
255 which is also confirmed from the crystal structures. The presence of the OH stretching frequency
256 around 3100-3450 cm^{-1} in cationic complexes (**4-9**) suggests that the binding occurs through the
257 nitrogen atom. In addition, the cationic metal complexes (**4-9**) displayed a strong intense band
258 around 838-849 cm^{-1} corresponding to the P-F stretching frequency of the counter ion [49].

259 In the ^1H NMR spectra of the complexes the signals for the aromatic protons of the ligand
260 was observed in the downfield region around 7.32-9.50 ppm. The shift of the ligand resonance
261 signals clearly indicates the coordination of the ligand to the metal ion. The disappearance of the
262 OH proton signal in the neutral complexes (**1-3**) as compared to the free ligand at 13.02 ppm
263 indicates the deprotonation of the hydroxyl proton. The OH proton resonance for complexes (**7-**
264 **9**) was observed as singlet around 11.3-11.9 ppm respectively. Besides these resonance signals
265 for the aromatic part of the ligand complexes (**1, 4** and **7**) displayed an unusual pattern of signal
266 for the *p*-cymene moiety. The aromatic proton signal for the *p*-cymene ligand showed four
267 doublets for complexes (**1**) and (**4**) at around 5.60-6.19 ppm and three doublets for complex (**7**)

268 around 5.64-6.06 ppm instead of two doublets in the starting metal precursor. And also methyl
269 protons of isopropyl group displayed two doublets for complex (4) and (7) and one doublet of
270 doublet for complex (1) around 1.01-1.18 ppm instead of one doublet in the metal precursor.
271 This surprising pattern of signals is due to desymmetrization of the *p*-cymene ligand upon
272 coordination of the oxime ligand and these results are in good agreement with similar reported
273 complexes [50]. Complexes (1, 4 and 7) displayed septet and singlet around 2.07-2.75 ppm
274 corresponding to the methine protons of the isopropyl group and methyl group of the *p*-cymene
275 ligand. The methyl proton resonance for complexes (8) and (9) was observed as a singlet at 2.56
276 and 2.58 ppm. In addition, to all these signals a strong peak for the Cp*Rh complexes (2, 5 and
277 8) and the Cp*Ir complexes (3, 6 and 9) was observed between 1.59-1.78 ppm for the methyl
278 protons of the pentamethylcyclopentadienyl ligand.

279 In the mass spectra of the neutral complexes (1-3), the molecular ion peak was observed
280 as (M+H)⁺ ion peak at m/z: 417.0302, m/z: 420.0451 and m/z: 510.0824 respectively. Whereas
281 the mass spectra of the cationic complexes (4-9) displayed their molecular ion peaks at m/z:
282 469.0652, m/z: 471.0721, m/z: 561.1283, m/z: 413.0118, m/z: 415.0131 and m/z: 505.0761
283 which corresponds to the [M-PF₆]⁺ ion. The mass spectra values of the complexes strongly
284 support the formation of the complexes.

285 The absorption spectra of the complexes were recorded in acetonitrile at 10⁻⁴ M
286 concentration at room temperature and the plot is shown in (Figure S1). The electronic spectra of
287 the complexes display absorption band in the higher energy region around 230-305 nm which
288 can be assigned as ligand centered π - π^* and n- π^* transition [51]. The low spin Ru(II), Rh(III) and
289 Ir(III) complexes provides filled $d\pi$ (t_{2g}) orbitals of proper symmetry which can interact with low
290 lying π^* orbitals of the ligand. Therefore a metal to ligand charge transfer (MLCT) band is

291 expected in their absorption spectra. The bands in the lower energy region around 350-380 nm
292 can be assigned as metal to ligand charge transfer (MLCT) $d\pi(M)$ to $\pi^*(L)$ transition [52].

293 3.3. Molecular structures of complexes

294 The molecular structures of some of the respective complexes were established by single
295 crystal X-ray analysis. Suitable single crystals were attached to a glass fiber and transferred into
296 the Oxford Diffraction Xcalibur Eos Gemini diffractometer. The crystallographic details and
297 structure refinement details are summarized in Table 1. The geometrical parameters around the
298 metal atom involving ring centroid are listed in Table 2. Complex (1) crystallized in
299 orthorhombic system with space group $Pca2_1$. Complexes (2, 3 and 8) crystallized in monoclinic
300 crystal system with space group $P2_1/c$ whereas complexes (4) and (7) crystallized with $P2_1/n$ and
301 $P2_1/m$ space group in monoclinic crystal system. Complex (5) crystallized in triclinic system
302 with space group $P\bar{1}$.

303 The molecular structures of the complexes revealed a typical three legged “piano stool”
304 geometry about the metal center with the metal atom coordinated by the arene/Cp* ring in a $\eta^6/$
305 η^5 manner, two nitrogen donor atoms from chelating ligand in a bidentate $\kappa^2 NN'$ fashion and one
306 chloride atom. The metal atom in these complexes is situated in a pseudo-octahedral arrangement
307 with the ligand coordinating through the pyridine and oxime nitrogen atom forming a five
308 membered metallocyclic ring. The bite angle values N(1)-Ru(1)-N(2) in ruthenium complexes
309 are 77.81(13) (1), 75.66(7) (4) and 78.0(10) (7). The average Ru-C distances in complexes (1)
310 and (4) are almost equal 2.203 and 2.205 Å, while in complex (7) the Ru-C distance is 2.179 Å.
311 The Ru-centroid of the arene ring distances in complexes (1) and (4) are equal 1.696 Å while in
312 complex (7) it is slightly longer 1.728 Å. The bite angle values N(1)-M(1)-N(2) in rhodium and
313 iridium complexes are 78.06(16) (2), 78.0(3) (3), 74.92(11) (5) and 75.16(15) (8). The average

314 M-C distances (where M = Rh/Ir) are {2.165 (**2**), 2.170 (**3**), 2.157 (**5**) and 2.149 (**8**) Å} while the
315 distance between the metal to centroid of the Cp* ring is found to be in the range of 1.775-1.803
316 Å respectively. The M-N and M-Cl bond distances (where M = Ru, Rh and Ir) in all these
317 complexes are found to be in close agreement with previously reported values for ruthenium,
318 rhodium and iridium complexes with NN' donor ligands [53]. Surprisingly, the molecular
319 structures of complexes (**1**, **2** and **3**) revealed the deprotonation of the oxime hydrogen
320 generating an anionic charge on oxime-O. This anomalous behavior of deprotonation of the
321 oxime hydrogen is not surprising as the presence of electron withdrawing cyano group increases
322 the acidity of the oxime fragment. It was further observed that the anionic charge on the oxime-O
323 was delocalized over the 2-pyridyl cyanoxime moiety. This is supported by the oximate C(6)-
324 N(2) {1.330(5) (**1**), 1.334(7) (**2**) and 1.360(11) (**3**) Å} and N(2)-O(1) {1.271(4) (**1**), 1.262(5) (**2**)
325 and 1.254(9) (**3**) Å} bond lengths which is slightly larger and smaller than the corresponding C-
326 N {1.287(2) Å} and N-O {1.367(2) Å} bond in the free ligand indicating their partial double
327 bond character and delocalization of the anionic charge (Scheme-1) [54]. These results are
328 further supported by the theoretical calculations as well (Table S1). A similar pattern of
329 delocalization of charge was reported for the cyclometalated iridium complex [Ir(ppy)₂(pyald)]
330 (ppy = 2-phenylpyridine, pyald = 2-pyridinealdoxime) where the anionic charge was delocalized
331 over the pyridine aldoxime moiety [55]. The positive charge of the ruthenium atom in complex
332 (**1**) is balanced by one negative charge from chloride ion and one negative charge from the
333 oxime-O. Similarly in complexes (**2**) and (**3**), the positive charge of the metal atom is balanced
334 by one anionic charge from Cp* ligand, one chloride ion and anionic oxime-O.

335 Further the crystal structure of complex (**1**) displayed three different types of
336 intermolecular hydrogen bonding; the first between the anionic oxime-O and hydrogen atom

337 from pyridine (2.393 Å), the second between the oxime-O and methine hydrogen (2.383 Å) and
338 third from the aromatic hydrogen of *p*-cymene ligand (2.531 Å). Also C-H····Cl (2.848 Å)
339 interaction between the chloride atom and H-atom of pyridine ring (Figure S2) has been
340 observed. Crystal structure of complex (2) exhibits two different types of C-H····Cl (2.813 and
341 2.902 Å) interactions between the chloride atom attached to metal and H-atom of Cp* group and
342 pyridine and also C-H···· π (2.904 Å) interaction was observed between the methyl-H atom and
343 Cp* group (Figure S3). The crystal structure of complex (3) is stabilized by C-H···· π (2.756 Å)
344 interaction between the methyl-H atom and Cp* group and C-H····Cl (2.917 Å) interaction
345 between chloride atom and methyl H atom of Cp*. It also exhibits two types of intermolecular
346 hydrogen bonding C-H····O (2.713 Å) between the anionic oxime-O and methyl-H of Cp* and
347 C-H····N (2.689 Å) interaction between nitrogen atom of cyano group and pyridine-H atom
348 (Figure S4). The crystal packing of complex (4) and (5) forms a dimeric unit via weak
349 intermolecular C-H····O (2.700 and 2.848 Å) and O-H····Cl (2.228 and 2.245 Å) interactions
350 between the methyl-H atom of Cp* and oxime-O and oxime-H atom and chloride atom attached
351 to metal ion (Figure S5). Further the crystal structure of complex (8) crystallized with one water
352 molecule which forms four different types of intermolecular hydrogen bonding the first between
353 the hydrogen atom of water molecule and chloride atom O-H····Cl (2.807 Å), the second
354 between the fluorine atom of counter ion PF₆ and H-atom of water molecule O-H····F (2.319 Å),
355 the third between the O-atom and H-atom of Cp* group C-H····O (2.507 Å) and the last between
356 the O-atom and H-atom of oxime moiety O-H····O (1.829 Å) (Figure S6). These weak
357 interactions play an important role in the formation of supramolecular motifs.

358 3.4. Chemosensitivity studies

359 The oximato and oxime metal complexes (**1-9**) were tested for their *in vitro* activity
360 against two cancer cell lines HT-29 (human colorectal cancer) and MIAPaCa-2 (human
361 pancreatic cancer) using the MTT assay. The response of the cell line HT-29 and MIAPaCa-2 to
362 the test complexes (**1-9**) and cisplatin is presented in graphical form in Figure 4 and in tabular
363 form in Table 3. Complexes (**1**) and (**8**) were found to be inactive against both the cell line with
364 IC_{50} values $> 100 \mu\text{M}$. Complexes (**4**) and (**5**) were found to be less active against HT-29 cell
365 line whereas complex (**4**) was found to be more active against MIAPaCa-2 cell line. In contrast
366 complexes (**2**) and (**7**) displayed moderate activity against both cell lines with IC_{50} value in the
367 range of 8.28 to 23.74 μM . However, among all the ruthenium, rhodium and iridium complexes,
368 the iridium complexes (**3**), (**6**) and (**9**) with cyano, phenyl and methyl substituted oximes
369 displayed high cytotoxicity. The iridium complexes were found to be highly active against HT-
370 29 cancer cell line with IC_{50} values in the range of 5.82 to 10.54 μM . Also, the iridium
371 complexes exhibits high potency against MIAPaCa-2 cell line with IC_{50} values ranging from
372 2.89 to 9.65 μM . However among all the iridium complexes, the iridium oximato compound (**3**)
373 with cyano substituent was found to be the most potent towards MIAPaCa-2 cell line ($IC_{50} =$
374 $2.87 \pm 0.26 \mu\text{M}$) with IC_{50} value comparable to that of cisplatin ($IC_{50} = 2.84 \pm 2.05 \mu\text{M}$). This
375 high remarkable activity of the iridium based complexes suggests that the presence of the
376 substituent in the chelating ligand plays a crucial role and affects the cytotoxicity [8]. This study
377 demonstrates that the cytotoxicity of the complexes can be finely tuned by changing the nature
378 and position of the substituent in the chelating ligand without changing the arene systems.

379 3.5. *Optimized structural geometry*

380 The comparison of the geometric parameters (selected bond lengths and bond angles) of
381 the optimized structures and the crystal structures of the complexes (**1-9**) are listed in Table S1.

382 The calculated bond lengths and the bond angles of the complexes are in good agreement with
383 the experimental data indicating the reliability of the theoretical method (B3LYP/6-
384 31G**/LanL2DZ) used in the present study. It should be noted that a slight discrepancy from the
385 experimental value in N(2)-Ru(1)-Cl(1), N(1)-Ru(1)-Cl(1) and N(2)-Rh(1)-Cl(1) bond angle for
386 complexes (1), (4) and (8) has been observed (Table S1).

387 3.6. *Molecular electrostatic potential (MESP)*

388 MESP is an important quantity to understand sites for electrophilic attack and
389 nucleophilic attack as well as hydrogen bond interactions [56, 57]. The MESP diagram for all the
390 complexes are shown in Figure 5. The red region represents the negative electrostatic potential,
391 which is related to the nucleophilic reactivity whereas the blue regions represents the positive
392 electrostatic potential and is related to the electrophilic reactivity. The red regions in complexes
393 containing 2-pyridyl cyanoxime and 2-pyridyl phenyloxime does not change much drastically,
394 but in complexes containing 2-thiazolyl methyloxime, the intensity of red color decreases
395 slightly in complexes (8) and (9) as compared to complex (7).

396 3.7. *Charge Distribution*

397 The charges on the selected atoms as obtained from NBO analysis are listed in Table S2.
398 The charge on the metal (Ru, Rh and Ir) for complexes (1-9) ranges between -0.028 e (complex
399 7) and 0.0248 e (complex 3), which are less than their formal charges of +2 (Ru) and +3 (Rh/Ir).
400 Moreover, as indicated in Table S2, the negative charge on the N1 decreases in all the complexes
401 as compared to their charge in isolated ligands. These results confirm that the ligands transfer
402 their negative charges to the metal on complex formation. The charge on the chloride atom for
403 all the complexes ranges between -0.342 e and -0.406 e. It should be noted that the negative
404 charges on chloride for ruthenium complexes are comparatively lower whereas it is higher for
405 rhodium and iridium complexes. These lowering of charges in ruthenium complexes are the

406 reflection of the negative charges on ruthenium complex (1) and (7) and very small positive
407 charge of 0.002 e on Ru in complex (4). As observed from the experimental results, that in the
408 neutral complexes (1, 2 and 3) the anionic charge on oxime-O was delocalized over the 2-pyridyl
409 cyanoxime moiety, therefore we further tried to justify these results with theoretical data as well.
410 In isolated ligand, 2-pyridyl cyanoxime, the charges on the O1, N2 and C6 are found to be -
411 0.545, -0.037 and 0.062 e. On complex formation, the negative charges on the O1 and N2
412 decreases and attains a value of -0.381, -0.387, -0.403 e and 0.159, 0.126, 0.107 e respectively,
413 whereas C6 attains negative charges of -0.050, -0.036 and -0.036 e (Table S2). These results
414 confirm that the anionic charge on the oxime-O is delocalized on complex formation. Moreover,
415 as seen from the bond lengths values (Table 2), on complex formation, the N2-O1 bond is
416 shortened and attains a partial double bond character whereas the N2-C6 bond is elongated as
417 compared to the bonds in isolated ligand.

418 3.8. Frontier Molecular Orbital and Absorption spectra

419 It is well known that the frontier molecular orbitals (HOMO and LUMO) help in
420 characterizing the electron donating and electron accepting ability of a molecule. Moreover, the
421 HOMO-LUMO energy gap has been utilized as an important parameter to understand the
422 reactivity of a molecule. A lower HOMO-LUMO gap means lesser stability and higher reactivity
423 whereas for higher HOMO-LUMO gap, it is the reverse case. The details of the frontier
424 molecular orbitals are shown in Figure 6 where the red and the green regions represent the
425 positive and the negative phase respectively. The energy gap is least for complex (6) whereas it
426 is highest for complex (8). It should be noted that the energy gap is less for the complexes
427 containing 2-pyridyl phenyloxime indicating its less stability and greater reactivity as compared
428 to the complexes containing ligand 2-pyridyl cyanoxime and 2-thiazolyl methyloxime. The %
429 composition of molecular orbital analysis as shown in Table S3, predicts that for the complexes

430 containing 2-pyridyl cyanoxime (complexes **1**, **2** and **3**), the maximum percentage of HOMO i.e.
431 42%, 35% and 39% is located on the ligand itself. The same case can be encountered for
432 complexes (**7**) and (**8**) as well whereas for complexes (**4**), (**6**) and (**9**) most percentage of HOMO
433 is located on the metal (Table S3). On the other hand, the LUMO is located mainly on the ligand
434 for almost all the complexes except for complex (**2**), where it is located on the Rh metal (about
435 37%).

436 The electronic absorption spectra were calculated using the TD-DFT method in
437 acetonitrile solvent employing PCM model. The calculated and the experimental absorption data,
438 HOMO-LUMO energy gaps, and the character of electronic transitions are listed in Table 4. The
439 H→L transitions for complexes (**1**), (**3**), (**7**) and (**8**) occurring at 492, 468, 450 and 485 nm
440 corresponds to ILCT character, for complexes (**4**), (**6**) and (**9**) at 453, 464 and 463 nm
441 corresponds to MLCT character whereas for complexes (**2**) and (**5**) at 512.44 and 477 nm
442 corresponds to LMCT and LLCT character. These MLCT character can be assigned as
443 $d\pi(M)\rightarrow\pi^*(L)$ transitions, ILCT character are for $\pi\rightarrow\pi^*$ transitions and LLCT for $P\pi(Cl)\rightarrow\pi^*(L)$
444 transitions. In agreement with the experimental results, few MLCT transitions has also been
445 observed at 357 nm (**4**), 359, 335 nm (**7**), 336 nm (**8**) and 350 nm (**9**). Further, few ILCT and
446 LLCT transitions have been observed between 230-304 nm which are in well agreement with the
447 experimental data.

448 4. Conclusion

449 In summary, we have successfully synthesized ruthenium, rhodium and iridium half-
450 sandwich oximate and oxime complexes. These complexes were full characterized by various
451 spectroscopic studies and X-ray analysis. The ligands under study preferably bind to the metal in
452 a bidentate κ^2 NN' fashion using pyridine and oxime nitrogen atom. X-ray structure of

453 complexes (**1-3**) reveals the deprotonation of the oxime hydrogen atom leading to the formation
454 of neutral complexes. Chemosensitivity activity of the complexes carried out against HT-29 and
455 MIAPaCa-2 cancer cell lines displayed that some of the complexes are cytotoxic however
456 iridium-based complexes displayed more potency than ruthenium and rhodium complexes. In
457 particularly the neutral iridium oximate compounds possessed the highest activity among other
458 cationic iridium oxime complexes. Further, TD-DFT calculated absorption spectral data are in
459 well agreement with experimental results.

460 **Acknowledgements**

461 Sanjay Adhikari and Dipankar Sutradhar thanks UGC, New Delhi, India for providing financial
462 assistance in the form of university fellowship (UGC-Non-Net). We thank DST-PURSE
463 SCXRD, NEHU-SAIF, Shillong, India for providing Single crystal X-ray analysis and other
464 spectral studies. AKC thanks Computer center, NEHU, for computational facilities.

465 **Appendix A. Supplementary data**

466 CCDC **1486252** (1), **1486253** (2), **1486254** (3), **1486255** (4), **1486256** (5), **1486257** (7)
467 and **1486258** (8) contains the supplementary crystallographic data for this paper. These data can
468 be obtained free of charge via www.ccdc.cam.ac.uk/data_request/cif, by e-mailing
469 data_request@ccdc.cam.ac.uk, or by contacting The Cambridge Crystallographic Data Centre,
470 12, Union Road, Cambridge CB2 1EZ, UK; Fax: +44 1223 336033.

471 **References**

- 472 [1] A.A. Nazarov, C.G. Hartinger, P.J. Dyson, *J. Organomet. Chem.* 751 (2014) 251.
473 [2] B. Therrien, *Coord. Chem. Rev.* 253 (2009) 493.
474 [3] L. Ronconi, P.J. Sadler, *Coord. Chem. Rev.* 251 (2007) 1633.
475 [4] A.F.A. Peacock, P.J. Sadler, *Chem. Asian J.* 3 (2008) 1890.

- 476 [5] A.L. Noffke, A. Habtemariam, A.M. Pizarro, P.J. Sadler, *Chem. Comm.* 48 (2012)
477 5219.
- 478 [6] Y. Geldmacher, M. Oleszak, W.S. Sheldrick, *Inorg. Chim. Acta* 393 (2012) 84.
- 479 [7] G.Suss-Fink, *Dalton Trans.* 39 (2010) 1673.
- 480 [8] A.J. Millett, A. Habtemariam, I. Romero-canelon, G.J. Clarkson, P.J. Sadler,
481 *Organometallics*, 34 (2015) 2683.
- 482 [9] Z. Almodares, S.J. Lucas, B.D. Crossley, A.M. Basri, C.M. Pask, A.J. Hebden, R.M.
483 Philips, P.C. McGowan, *Inorg. Chem.* 53 (2014) 727.
- 484 [10] Y.K. Yan, M. Melchart, A. Habtemariam, P.J. Sadler, *Chem. Commun.* (2005) 4764.
- 485 [11] C.G. Hartinger, N. Metzler-Nolte, P.J. Dyson, *Organometallics*, 31 (2012) 5677.
- 486 [12] R.E. Morris, R.E. Aird, P.S. Murdoch, H. Chen, J. Cummings, N.D. Hughes, S.
487 Parsons, A. Parkin, G. Boyd, D.I. Jodrell, P.J. Sadler, *J. Med. Chem.* 44 (2001) 3616.
- 488 [13] M. Martinez-Alonso, N. Busto, F.A. Jalon, B.R. Manzano, J.M. Leal, A.M. Rodriguez,
489 B. Garcia, G. Espino, *Inorg. Chem.* 53 (2014) 11274.
- 490 [14] Z. Liu, A. Habtemariam, A.M. Pizarro, S.A. Fletcher, A. Kisova, O. Vrana, L. Salassa,
491 P.C.A. Bruijninx, G.J. Clarkson, V. Brabec, P.J. Sadler, *J. Med. Chem.* 54 (2011)
492 3011.
- 493 [15] A. Habtemariam, M. Melchart, R. Fernandez, S. Parsons, I.D.H. Oswald, A. Parkin,
494 F.P.A. Fabbiani, J.E. Davidson, A. Dawson, R.E. Aird, D.I. Jodrell, P.J. Sadler, *J. Med.*
495 *Chem.* 49 (2006) 6858.
- 496 [16] S.J. Lucas, R.M. Lord, A.M. Basri, S.J. Allison, R.M. Phillips, A.J. Blacker, P.C.
497 McGowana, *Dalton Trans.* 45 (2016) 6812.
- 498 [17] B. Lastra-Barreira, J. Diez, P. Crochet, I. Fernandez, *Dalton Trans.* 42 (2013) 5412.

- 499 [18] J.M. Hearn, I. Romero-Canelon, B. Qamar, Z. Liu, I. Hands-Portman, P.J. Sadler,
500 Chem. Biol. 8 (2013) 1335.
- 501 [19] H. Turkmen, I. Kani, B. Cetinkaya, Eur. J. Inorg. Chem. (2012) 4494.
- 502 [20] J. DePasquale, I. Nieto, L.E. Reuther, C.J. Herbst-Gervasoni, J.J. Paul, V. Mochalin. M.
503 Zeller, C.M. Thomas, A.W. Addison, E.T. Papish, Inorg. Chem. 52 (2013) 9175.
- 504 [21] N. Hofmann, L. Ackermann, J. Am. Chem. Soc. 135 (2013) 5877.
- 505 [22] (a) G. Gupta, S. Gloria, S.L. Nongbri, B. Therrien, K.M. Rao, J. Organomet. Chem. 696
506 (2011) 2014; (b) M. Kalidasan, S.H. Forbes, Y. Mozharivskyj, K.M. Rao, Inorg. Chim.
507 Acta 421 (2014) 218; (c) S. Sangilipandi, D. Sutradhar, K. Bhattacharjee, W.
508 Kaminsky, S.R. Joshi, A.K. Chandra, K.M. Rao, Inorg. Chim. Acta 441 (2016) 95.
- 509 [23] A. Chakravorty, Coord. Chem. Rev. 13 (1974) 1.
- 510 [24] C.W. Glynn, M.M. Turnbull, Trans. Met. Chem. 27 (2002) 822.
- 511 [25] N. Gerasimchuk, T. Maher, Inorg. Chem. 46 (2007) 7268.
- 512 [26] N. Gerasimchuk, A. Gamian, G. Glover, B. Szponar, Inorg. Chem. 49 (2010) 9863.
- 513 [27] C.J. Milios, T.C. Stamatatos, S.P. Perlepes, Polyhedron, 25 (2006) 134.
- 514 [28] A. Escuer, G. Vlahopoulou, S.P. Perlepes, F.A. Mautner, Inorg. Chem. 50 (2011) 2468.
- 515 [29] J. Esteban, M. Font-Bardia, J.S. Costa, S.J. Teat, A. Escuer, Inorg. Chem. 53 (2014)
516 3194.
- 517 [30] M. Watanabe, Y. Kashiwame, S. Kuwata, T. Ikariya, Eur. J. Inorg. Chem. (2012) 504.
- 518 [31] M. Watanabe, Y. Kashiwame, S. Kuwata, T. Ikariya, Chem. Lett. 39 (2010) 758.
- 519 [32] D.D. Perrin, W.L.F. Armarego, Purification of Laboratory Chemicals, fourth ed.,
520 Butterworths Heinemann, London, 1996.
- 521 [33] M.A. Bennett, T.N. Huang, T.W. Matheson, A.K. Smith, S. Ittel, W. Nickerson,

- 522 Inorg. Synth. 21 (1982) 74.
- 523 [34] C. White, A. Yates, P.M. Maitlis, D.M. Heinekey, Inorg. Synth. 29 (2007) 228.
- 524 [35] H. S. Jena, V. Manivannan, Inorg. Chim. Acta 394 (2013) 210.
- 525 [36] R.A. Hughes, S.P. Thompson, L. Alcaraz, C.J. Moody, J. Am. Chem. Soc. 127 (2005)
- 526 15644.
- 527 [37] G.M. Sheldrick, Acta Crystallogr. Sect. A 46 (1990) 467.
- 528 [38] G.M. Sheldrick, Acta Crystallogr. Sect. A 64 (2008) 112.
- 529 [39] L.J. Farrugia, J. Appl. Crystallogr. 32 (1999) 837.
- 530 [40] (a) A.L. Spek, PLATON, A Multipurpose Crystallographic Tool, Utrecht
- 531 University, Utrecht, The Netherlands, 2008; (b) A.L. Spek, J. Appl. Crystallogr. 36
- 532 (2003) 7.
- 533 [41] R.M. Phillips, P.B. Hulbert, M.C. Bibby, N.R. Sleigh, J.A. Double, Br. J. Cancer.
- 534 65 (1992) 359.
- 535 [42] A.D. Becke, J. Chem. Phys., 98, 7 (1993) 5648.
- 536 [43] C. Lee, W. Yang, R.G. Parr, Phys. Rev., B 37, 2 (1988) 785.
- 537 [44] E. Cancès, B. Mennucci, J. Tomasi, J. Chem. Phys. 107 (1997) 3032.
- 538 [45] A. E. Reed, L. A. Curtiss, F. Weinhold, Chem. Rev. 88 (1988) 899.
- 539 [46] M.E. Casida, in: J. M. Seminario (Ed.), Recent Developments and Applications in Modern
- 540 Density Functional Theory, Theoretical and Computational Chemistry, vol. 4, Elsevier,
- 541 Amsterdam, 1996.
- 542 [47] L. Skripnikov, Chemissian v4.36, A computer program to analyse and visualise quantum-
- 543 chemical calculations, 2015.
- 544 [48] M.J. Frisch et al., GAUSSIAN 09, Revision C.01, Gaussian, Inc., Walling-ford, CT 2009.

- 545 [49] K. Nakamoto, *Infrared and Raman Spectroscopy of Inorganic and Coordination*
 546 *Compounds*, fourth ed., Wiley, New York, 1986.
- 547 [50] J.M. Gichumbi, H.B. Friedrich, B. Omondi, *J. Organomet. Chem.* 808 (2016) 87.
- 548 [51] N. Mohan, S. Muthumari, R. Ramesh, *J. Organomet. Chem.* 807 (2016) 45.
- 549 [52] G. Gupta, S. Park, S. S. Lee, J. Kim, *Z. Anorg. Allg. Chem.* 637, 2011, 1516.
- 550 [53] (a) K.T. Prasad, B. Therrien, K.M. Rao, *J. Organomet. Chem.* 693 (2008) 3049; (b) G.
 551 Gupta, S. Gloria, B. Das, K.M. Rao, *J. Mol. Struc.* 979 (2010) 205; (c) J.M. Gichumbi,
 552 H.B. Friedrich, B. Omondi, *J. Mol. Catal. A: Chemical* 416 (2016) 29; (d) L.C.
 553 Matsinha, S.F. Mapolie, G.S. Smith, *Polyhedron* 53 (2013) 56.
- 554 [54] A.A. Mokhir, K.V. Domasevich, N.K. Dalley, X. Kou, N.N. Gerasimchuk, O.A.
 555 Gerasimchuk, *Inorg. Chim. Acta.* 284 (1999) 85.
- 556 [55] S. Pal, B.C. Singh, *Acta Crystallogr. E*69 (2013) m159.
- 557 [56] L. Xiao-Hong, C. Hong-Ling, Z. Rui-Zhou, Z. Xian-Zhou, *Spectrochim. Acta A: Mol. Biomol.*
 558 *Spectrosc.* 137 (2015) 321.
- 559 [57] Y. Wang, Q. Liu, T. Wang, H. Yuan, J. Lin and S. Luo, 150 (2015), 902.

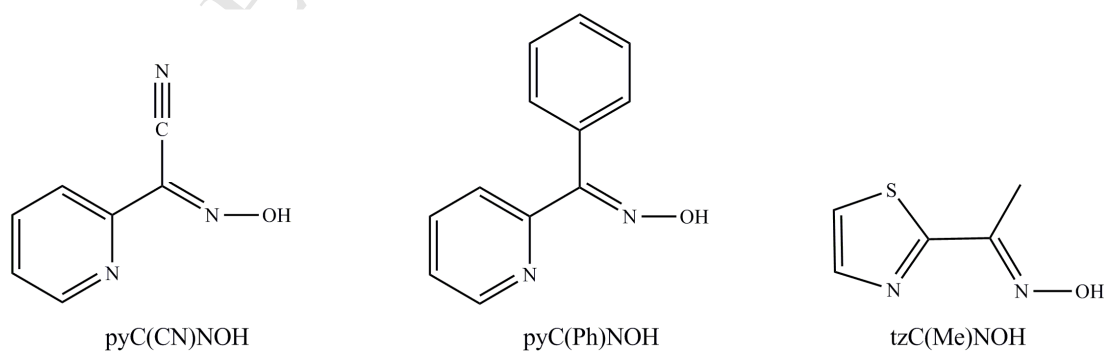
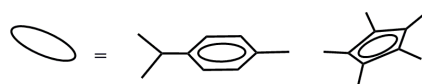
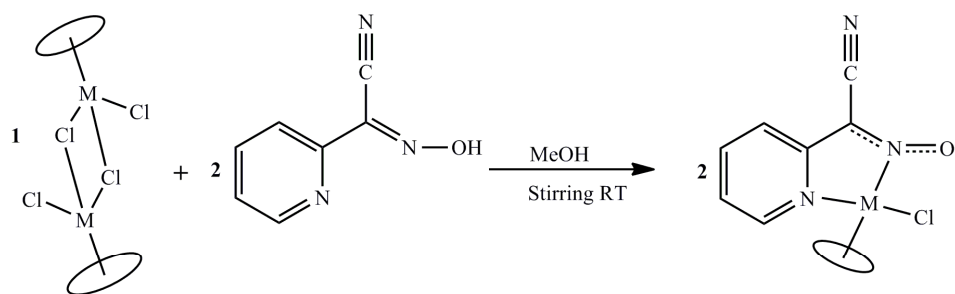


Chart-1



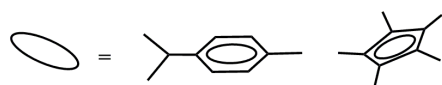
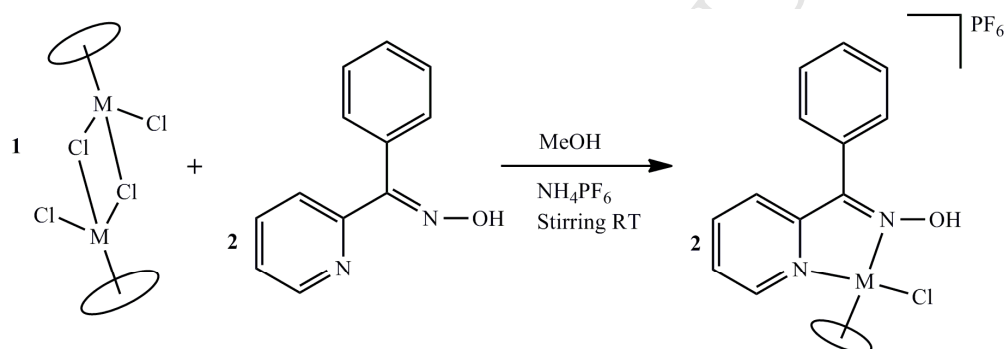
M = Ru (1) Rh (2) Ir (3)

566

567

568

Scheme-1 Preparation of neutral complexes (1-3)

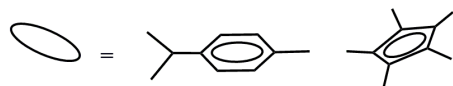
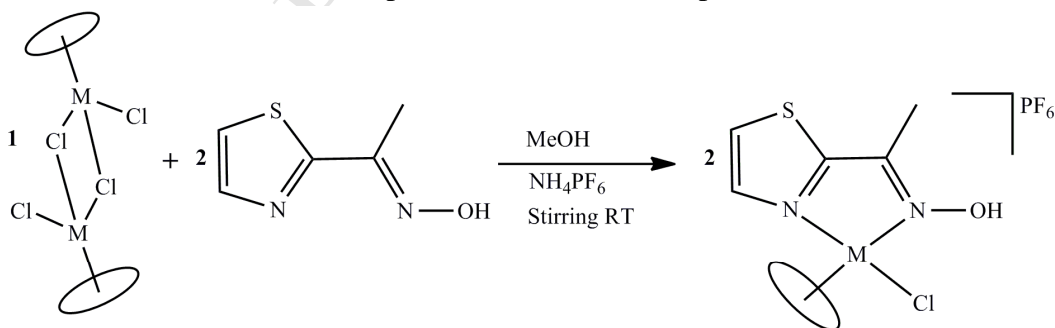


M = Ru (4) Rh (5) Ir (6)

569

570

Scheme-2 Preparation of cationic complexes (4-6)

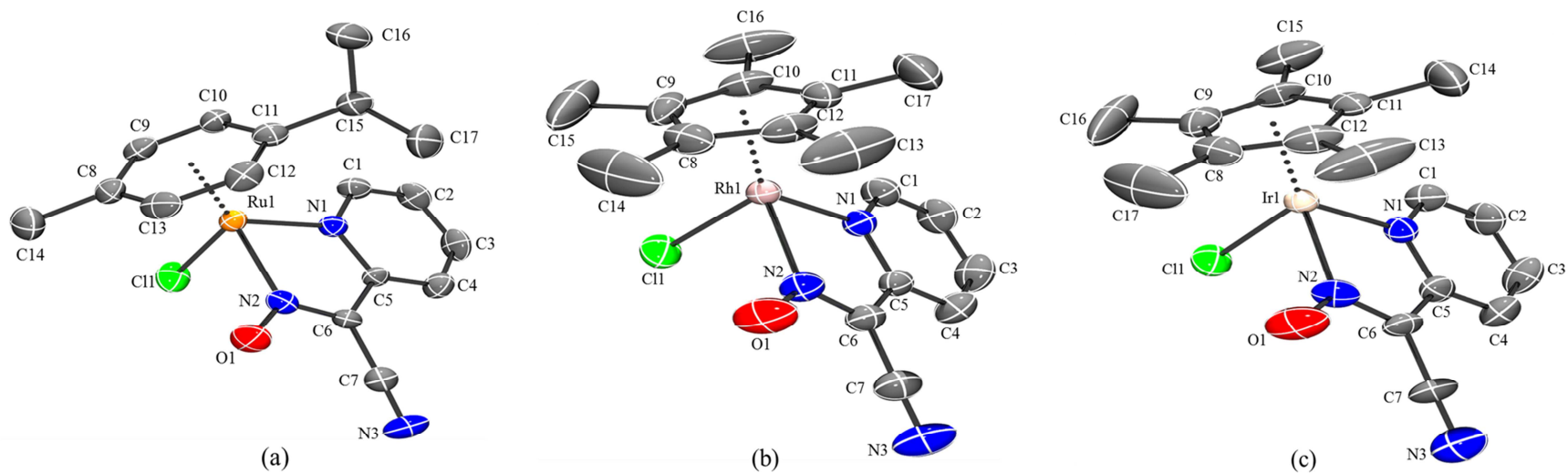


M = Ru (7) Rh (8) Ir (9)

571

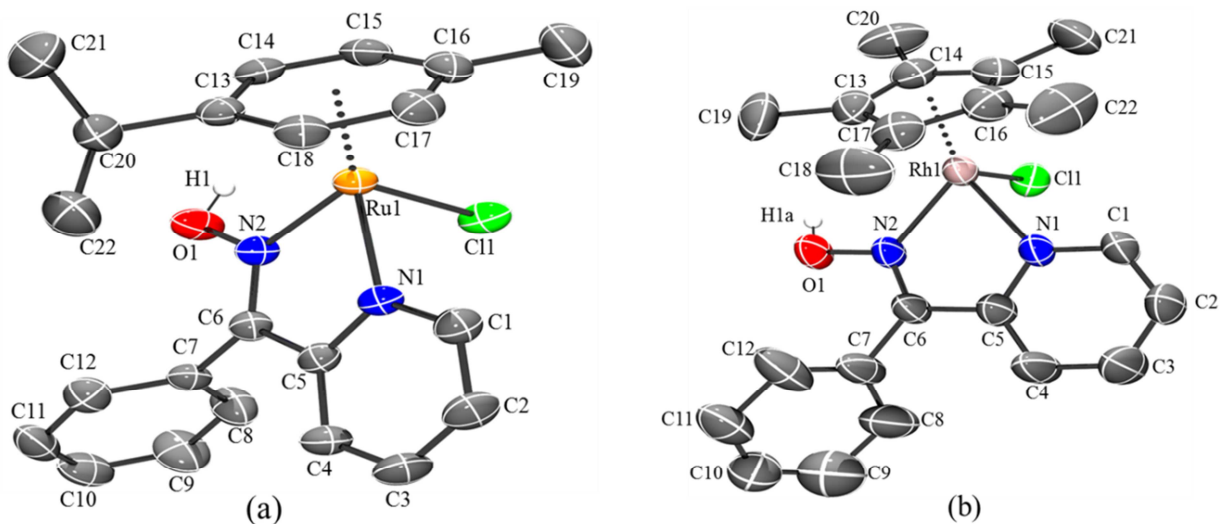
572

Scheme-3 Preparation of cationic complexes (7-9)



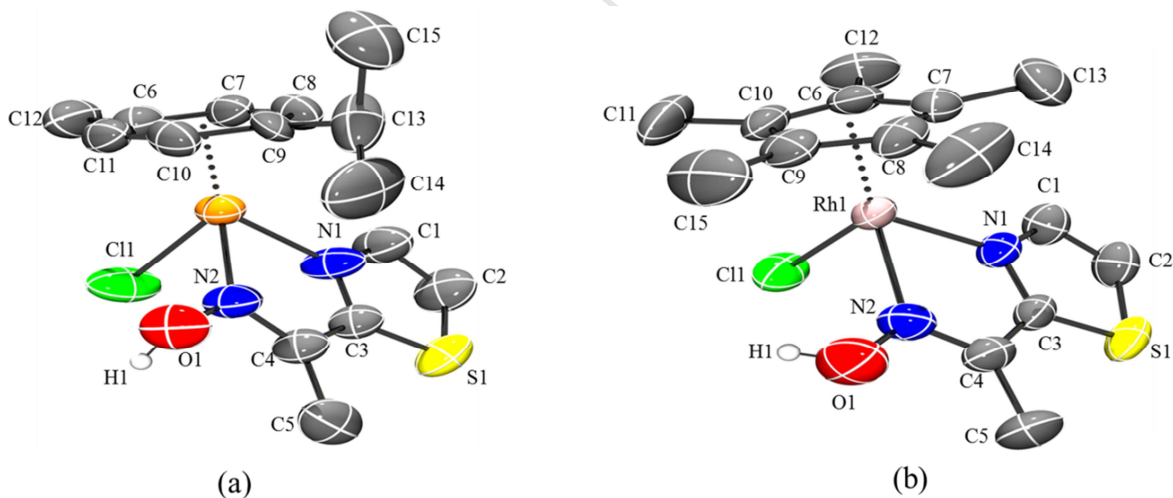
573

574 **Figure 1** (a) Ortep diagram of complex (1), (b) Ortep diagram of complex (2) and (c) Ortep diagram of complex (3) with 50%
575 probability thermal ellipsoids. Hydrogen atoms are omitted for clarity.

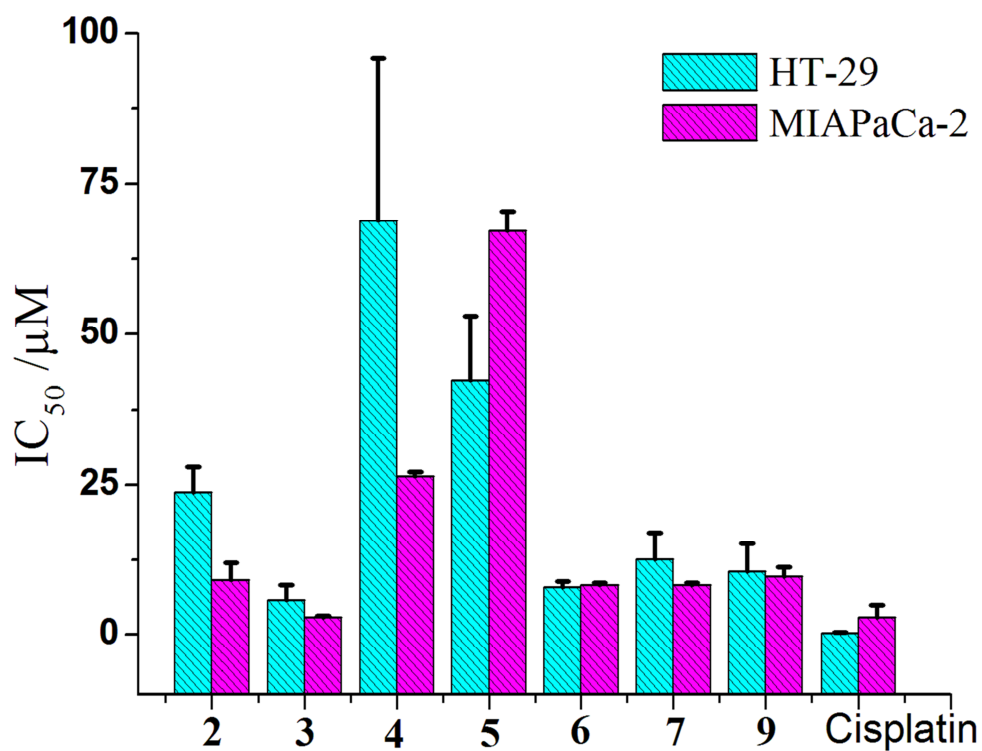


576
 577 **Figure 2** (a) Ortep diagram of complex (4) and (b) Ortep diagram of complex (5) with 50%
 578 probability thermal ellipsoids. Counter ions and hydrogen atoms (except on O1) are omitted for
 579 clarity.

580

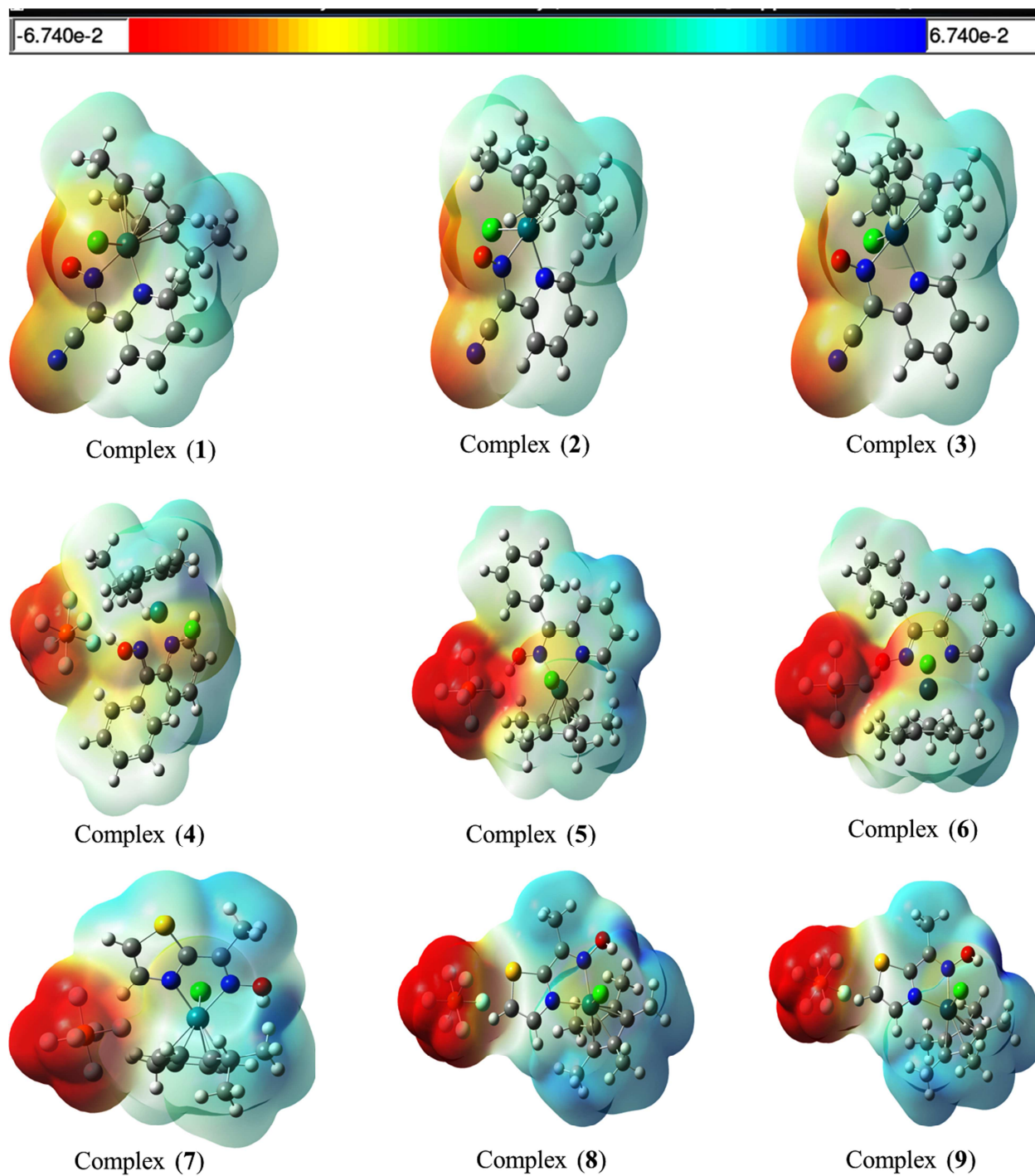


581
 582 **Figure 3** (a) Ortep diagram of complex (7) and (b) Ortep diagram of complex (8) with 50%
 583 probability thermal ellipsoids. Counter ions and hydrogen atoms (except on O1) are omitted for
 584 clarity.



585

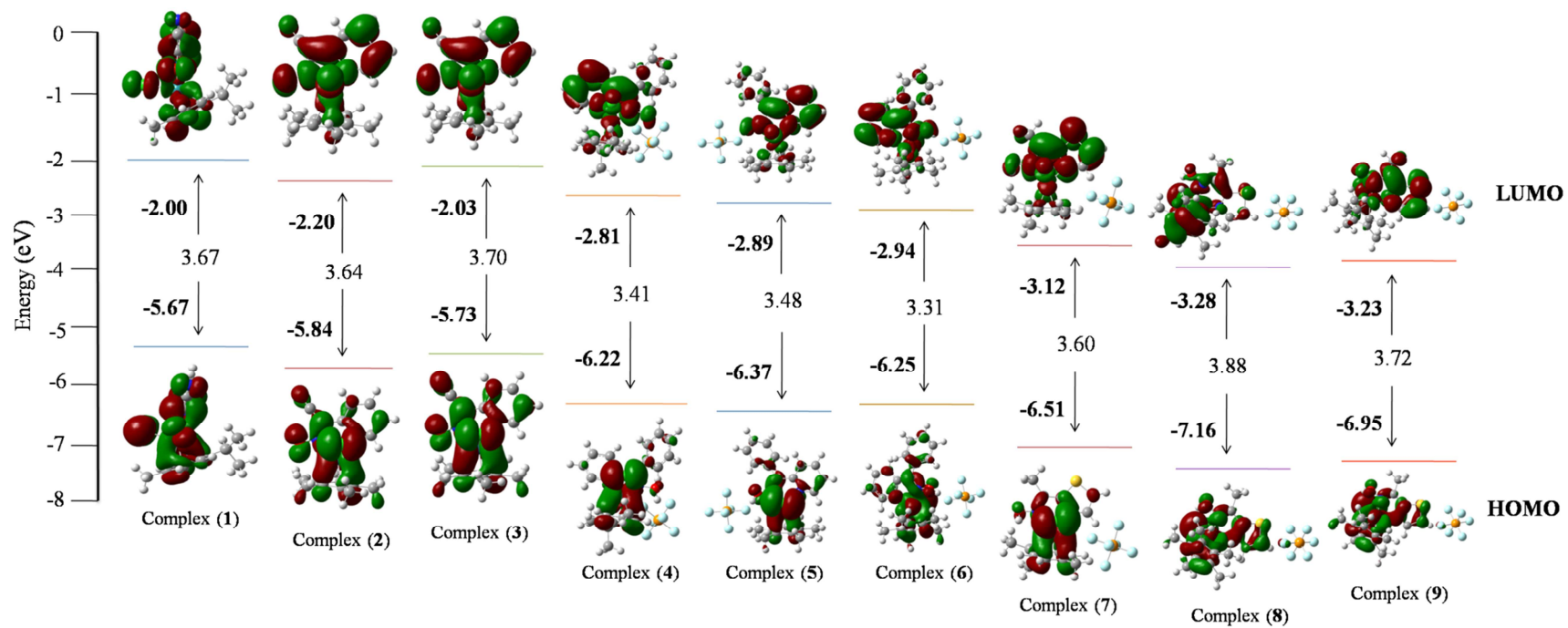
586 **Figure 4** Response of HT-29 (human colorectal cancer) and MIAPaCa-2 (human pancreatic
587 cancer) to compounds and cisplatin. Cell was exposed to compounds (1-9) for 96 hours. Each
588 value represents the mean \pm standard deviation from three independent experiments.



589

590

Figure 5 Molecular electrostatic potential diagrams for complexes (1-9).



591

592

Figure 6 HOMO, LUMO energies and their energy gaps of complexes (1-9).

593 Table 1 Crystal data and structure refinement parameters of complexes.

Compounds	[1]	[2]	[3]	[4]PF ₆	[5]PF ₆	[7]PF ₆	[8]PF ₆ ·H ₂ O
Empirical formula	C ₁₇ H ₁₈ ClN ₃ ORu	C ₁₇ H ₁₉ ClN ₃ ORh	C ₁₇ H ₁₉ ClN ₃ OIr	C ₂₂ H ₂₄ ClF ₆ N ₂ OPRu	C ₂₂ H ₂₅ ClF ₆ N ₂ OPRh	C ₁₅ H ₂₀ ClF ₆ N ₂ OPRuS	C ₁₅ H ₂₃ ClF ₆ N ₂ O ₂ PRhS
Formula weight	416.86	419.71	509.00	613.92	616.77	557.88	578.74
Temperature (K)	292(2)	291(2)	295(2)	292(2)	296(2)	291(2)	295(2)
Wavelength (Å)	0.71073	0.71073	0.71073	0.71073	0.71073	0.71073	0.71073
Crystal system	Orthorhombic	Monoclinic	Monoclinic	Monoclinic	Triclinic	Monoclinic	Monoclinic
Space group	<i>Pca</i> 2 ₁	<i>P</i> 2 ₁ / <i>c</i>	<i>P</i> 2 ₁ / <i>c</i>	<i>P</i> 2 ₁ / <i>n</i>	<i>P</i> <i>T</i>	<i>P</i> 2 ₁ / <i>m</i>	<i>P</i> 2 ₁ / <i>c</i>
a (Å)/α (°)	14.9960(5)/90	8.3023(9)/90	8.3165(6)/90	9.0701(4)/90	9.0597(5)/67.455(5)	10.5576(7)/90	12.6553(5)/90
b (Å)/β (°)	7.8142(2)/90	27.612(2)/112.173(12)	27.5547(13)/112.388(7)	14.1127(6)/98.340(4)	12.7557(7)/82.956(5)	9.3658(7)/104.388(7)	10.8936(4)/98.858(4)
c (Å)/γ (°)	14.6872(4)/90	8.1421(8)/90	8.2007(5)/90	19.6319(9)/90	13.2635(8)/87.886(5)	13.2319(10)/90	16.3323(6)/90
Volume (Å ³)	1721.07(9)	1728.5(3)	1737.61(18)	2486.38(19)	1404.86(14)	1267.34(16)	2224.75(15)
Z	4	4	4	4	2	2	4
Density (calc) (Mg/m ³)	1.609	1.613	1.946	1.640	1.458	1.462	1.728
Absorption coefficient (μ) (mm ⁻¹)	1.073	1.149	7.844	0.865	0.815	0.919	1.117
F(000)	840	848	976	1232	620	556	1160
Crystal size (mm ³)	0.24 x 0.19 x 0.09	0.24 x 0.19 x 0.08	0.29 x 0.25 x 0.02	0.29 x 0.24 x 0.12	0.21 x 0.19 x 0.15	0.36 x 0.25 x 0.23	0.25 x 0.21 x 0.19
Theta range for data collection	3.05 to 28.74°	3.08 to 28.74°	3.03 to 28.73°	3.07 to 29.07°	3.22 to 29.12°	3.58 to 28.93°	3.14 to 29.01°
Index ranges	-20<h<=16, -10<k<=9, -17<l<=18	-6<h<=11, -36<k<=36 -10<l<=10	-11<h<=11, -30<k<=36, -10<l<=5	-10<h<=12, -18<k<=10, -26<l<=17	-11<h<=11, -16<k<=11, -17<l<=17	-12<h<=14, -11<k<=12, -10<l<=17	-13<h<=15, -12<k<=13, -22<l<=20
Reflections collected	6209	8785	9093	9847	9798	4790	8932
Independent reflections	3438 [R(int) = 0.0311]	3956 [R(int) = 0.0602]	3978 [R(int) = 0.0494]	5682 [R(int) = 0.0186]	6373 [R(int) = 0.0329]	3037 [R(int) = 0.0230]	5071 [R(int) = 0.0261]
Completeness to theta = 25.00°	99.7 %	99.5 %	99.6 %	99.6 %	99.5 %	98.3 %	99.5 %
Absorption correction	Semi-empirical from equivalents	Semi-empirical from equivalents	Semi-empirical from equivalents	Semi-empirical from equivalents	Semi-empirical from equivalents	Semi-empirical from equivalents	Semi-empirical from equivalents
Max. And min. transmission	0.9096 and 0.7828	0.9137 and 0.7700	0.8589 and 0.2094	0.9033 and 0.7875	0.8875 and 0.8474	0.8164 and 0.7331	0.8159 and 0.7677
Refinement method	Full-matrix least-squares on F ²	Full-matrix least-squares on F ²	Full-matrix least-squares on F ²	Full-matrix least-squares on F ²	Full-matrix least-squares on F ²	Full-matrix least-squares on F ²	Full-matrix least-squares on F ²
Data/restraints/parameters	3438/1/211	3956/0/213	3978/30/213	5682/0/311	6373/136/412	3037/172/229	5071/3/275
Goodness-of-fit on F ²	1.00	1.057	1.085	1.090	1.059	1.005	1.049
Final R indices [I>2sigma(I)]	R1 = 0.0322, wR2 = 0.0498	R1 = 0.0566, wR2 = 0.0966	R1 = 0.0526, wR2 = 0.1118	R1 = 0.0331, wR2 = 0.0728	R1 = 0.0473, wR2 = 0.1153	R1 = 0.0524, wR2 = 0.1426	R1 = 0.0475, wR2 = 0.1064
R indices (all data)	R1 = 0.0425, wR2 = 0.0526	R1 = 0.1081, wR2 = 0.1077	R1 = 0.0713, wR2 = 0.1217	R1 = 0.0426, wR2 = 0.0777	R1 = 0.0649, wR2 = 0.1241	R1 = 0.0640, wR2 = 0.1540	R1 = 0.0706, wR2 = 0.1211
Largest diff. peak and hole (e.Å ⁻³)	0.583 and -0.461	0.790 and -0.865	2.329 and -1.955	0.377 and -0.519	0.449 and -0.350	0.871 and -0.857	0.734 and -0.393
CCDC No.	1486252	1486253	1486254	1486255	1486256	1486257	1486258

594 Structures were refined on F_0^2 : $wR_2 = [\sum[w(F_0^2 - F_c^2)^2] / \sum w(F_0^2)^2]^{1/2}$, where $w^{-1} = [\sum(F_0^2) + (aP)^2 + bP]$ and $P = [\max(F_0^2, 0) + 2F_c^2]/3$

595 Table 2 Selected bond lengths (Å) and bond angles (°) of complexes.

Complex	1	2	3	4	5	7	8
M(1)-CNT	1.696	1.799	1.803	1.696	1.788	1.728	1.775
M(1)-N(1)	2.073(3)	2.093(4)	2.084(7)	2.0587(18)	2.103(3)	2.09(2)	2.108(3)
M(1)-N(2)	2.028(3)	2.065(4)	2.039(7)	2.0854(19)	2.102(3)	2.08(3)	2.131(4)
M(1)-Cl(1)	2.3897(11)	2.3870(16)	2.391(2)	2.4191(7)	2.4225(10)	2.415(2)	2.3991(12)
M(1)-C _{ave}	2.203	2.165	2.170	2.205	2.157	2.179	2.149
N(2)-O(1)	1.271(4)	1.262(5)	1.254(9)	----	----	----	----
N(2)-C(6)	1.330(5)	1.334(7)	1.360(11)	----	----	----	----
N(1)-M(1)-N(2)	77.81(13)	78.06(16)	78.0(3)	75.66(7)	74.92(11)	78.0(10)	75.16(15)
N(1)-M(1)-Cl(1)	85.22(9)	87.07(13)	84.8(2)	85.10(6)	87.58(9)	88.4(5)	88.51(10)
N(2)-M(1)-Cl(1)	84.87(9)	86.72(14)	85.6(2)	84.20(5)	89.30(9)	81.1(6)	89.14(11)
N(1)-M(1)-CNT	132.9	132.5	133.8	132.0	129.6	132.3	128.6
N(2)-M(1)-CNT	130.6	130.4	131.2	131.5	130.5	133.0	132.4
Cl(1)-M(1)-CNT	127.3	125.5	125.7	129.2	127.7	127.8	126.3

596 CNT represents the centroid of the arene/Cp* ring; C_{ave} represents the average bond distance of
 597 the arene/Cp* ring carbon and metal atom.

598 Table 3 Response of HT-29 (human colorectal cancer) and MIAPaCa-2 (human pancreatic
 599 cancer) to complexes (**1-9**) and cisplatin. Each value represents the mean ± standard deviation
 600 from three independent experiments.

Complexes	IC ₅₀ (μM)	
	HT-29	MIAPaCa-2
1	>100	>100
2	23.74 ± 4.25	9.16 ± 2.89
3	5.82 ± 2.41	2.87 ± 0.26
4	68.83 ± 27.0	26.42 ± 0.67
5	42.32 ± 10.69	67.18 ± 3.16
6	7.92 ± 1.00	8.35 ± 0.29
7	12.56 ± 4.45	8.28 ± 0.42
8	>100	>100
9	10.54 ± 4.73	9.65 ± 1.68
Cisplatin	0.25 ± 0.11	2.84 ± 2.05

601 IC₅₀ = concentration of the drug required to inhibit the growth of 50% of the cancer cells (μM).

602 Table 4 Energy gap, theoretical and experimental absorption bands, electronic transitions and
 603 dominant excitation character for various singlet states of the complexes (1-9) calculated with
 604 TD-DFT method.

The most important orbital excitations	Calculated λ (nm)	Energy gap E (eV)	Oscillator strength (f)	Dominant excitation Character	Experimental λ (nm)
Complex 1					
H→L	492.28	3.67	0.0021	L1→L1(ILCT)	
H-3→L	371.17	4.50	0.0025	L1→L1(ILCT)	370
H-1→L	362.01	3.93	0.0488	L1→L1(ILCT)	
H→L+3	304.45	4.61	0.1337	L1→L1(ILCT)	302
H→L+4	301.08	4.89	0.0161	L1→Cp*(LLCT)	
H-2→L+6	238.25	5.91	0.0034	Cl→L1(LLCT)	237
H-5→L+2	235.61	5.92	0.0485	Ru→L1(MLCT)	
Complex 2					
H→L	512.44	3.65	0.0046	L1→Rh(LMCT)	
H-2→L+2	364.41	4.59	0.0306	Cl→Rh(LMCT)	374
H→L+3	293.93	4.65	0.0438	L1→L1(ILCT)	289
H-6→L+1	253.61	5.77	0.1544	Rh→L1(MLCT)	255
Complex 3					
H→L	467.55	3.70	0.0036	L1→L1(ILCT)	
H-2→L	376.61	4.26	0.0523	Cl→L1(LLCT)	378
H-3→L+1	290.41	5.24	0.0192	L1→Ir(LMCT)	288
H-1→L+2	283.58	4.68	0.0903	L1→L1(ILCT)	
H-6→L+2	232.24	6.20	0.0153	Ir→L1(MLCT)	233
Complex 4					
H→L	452.56	3.42	0.0024	Ru→L2(MLCT)	
H-2→L	379.18	4.09	0.0245	L2→L2(ILCT)	376
H-1→L+2	357.48	4.46	0.0106	Ru→L2(MLCT)	
H-4→L+1	271.57	4.86	0.0021	L2→Ru(LMCT)	272
H-4→L+3	231.48	5.51	0.0180	L2→L2(ILCT)	233
Complex 5					
H→L	476.51	3.48	0.0093	Cl→L2(LLCT)	
H-1→L+2	357.91	4.27	0.1024	Cl→Ru(LMCT)	357
H-2→L	345.27	3.95	0.0105	Cl→L2(LLCT)	
H-6→L+1	267.72	5.28	0.0341	L2→Rh(LMCT)	266
Complex 6					
H→L	464.21	3.32	0.0223	Ir+Cl→L2(MLCT/ LLCT)	
H-1→L+1	352.62	4.52	0.0372	Cl→L2(LLCT)	360
H-7→L	294.49	5.07	0.0102	Ir→L2(MLCT)	296
H-3→L+1	290.68	5.13	0.0026	L2→L2(ILCT)	
Complex 7					
H→L	450.26	3.39	0.0038	L3→L3(ILCT)	

H-3→L	359.31	4.01	0.0091	Ru→L3(MLCT)	347
H-3→L+1	334.71	5.01	0.0036	Ru→L3(MLCT)	
H-4→L	293.24	5.59	0.0598	Ru→L3(MLCT)	297
H→L+3	291.42	5.30	0.0328	L3→Ru(LMCT)	
Complex 8					
H→L	484.85	3.87	0.0028	L3→L3(ILCT)	
H-1→L+2	345.81	4.52	0.0506	L3→L3(ILCT)	349
H-3→L	335.78	4.40	0.0238	Rh→L3(MLCT)	
H-3→L+2	285.07	4.73	0.0296	Rh→L3(MLCT)	287
H-8→L+1	229.87	5.27	0.0127	Rh→L3(MLCT)	
Complex 9					
H→L	463.13	3.72	0.0010	Ir→L3(MLCT)	
H-1→L+1	350.0	4.81	0.0182	Ir→L3(MLCT)	360
H-2→L	288.36	4.37	0.0250	L3→L3(ILCT)	

605

Highlights

- ❖ Neutral oximato and cationic oxime complexes of ruthenium, rhodium and iridium were isolated with electron withdrawing and electron donating substituted pyridyl oximes.
- ❖ DFT calculations demonstrate that the calculated values are in good agreement with the experimental data.
- ❖ Iridium based oximato and oxime complexes exhibited better activity than ruthenium and rhodium complexes.